Turbulence measurements from moving platforms

IEEE/OES Current, Waves, and Turbulence Measurement Workshop - 2015

J. Thomson, J. Talbert, A. de Klerk, S. Zippel, M. Guerra
Applied Physics Lab, University of Washington
Seattle, WA, USA

L. Kilcher
National Renewable Energy Laboratory
Boulder, CO, USA

***Abstract*—Two recent methods for making high-fidelity turbulence measurements from moving platforms are described and demonstrated. The first is a method for measuring profiles of near-surface turbulence from a wave-following 'SWIFT' buoy. The second is a method for measuring time series of turbulence from a submerged compliant mooring. Both approaches use coherent Doppler instruments and inertial motion units (IMUs). In the buoy method, wave motions (e.g., pitch, roll, and heave) are quantified via GPS and IMU measurements. These wave motions are not present in the turbulence observations, because buoy follows the wave orbital motion, and thus the turbulent velocities are processed in the wave-following reference frame. In the mooring method, IMU measurements track the mooring motions (e.g., strum and kiting) and these motions are removed in post-processing to obtain turbulent velocities in the fixed earth reference frame. These approaches successfully quantify turbulence in regions previously unavailable or limited by the noise and spatial aliasing of sampling from bottom-mounted platforms.**

I. Introduction

Many marine applications and oceanographic studies require in situ measurements of turbulence. Often these measurements are confounded by the presence of strong mean currents and wave orbital velocities. The goal then is to decompose the total velocity u into components

$$u = \bar{u} + \tilde{u} + u', \tag{1}$$

where $\bar{u}$ is the time mean velocity, $\tilde{u}$ are the wave orbital velocities, and u' are the turbulent fluctuations.

The choice of reference frame is central to this decomposition and interpretation of the velocity measurements. In a fixed frame (Eulerian sensor platform), the turbulence u' is advected past a sensor by both the mean flow $\bar{u}$ and the wave orbitals $\tilde{u}$ [1]. In a fluid-following frame (Lagrangian sensor platform), a sensor only measures turbulence at scales smaller than the platform [2]. A hybrid reference frame (compliant platform) is between these limits, and is characterized by a sensor platform that moves with some portion of the flow, but also is partially restricted. This hybrid reference frame can have scientific advantages, such as in sampling at the ocean surface, or can have practical advantages, such as in reducing the size and complexity of deployment platforms.

Recently, reference frame tracking has become feasible with the advent of high-quality Inertial Motion Units (IMUs) at moderate cost. Thus, turbulence measurements can be collected and adjusted for the reference frames of freely drifting buoys, compliant moorings, and other moving platforms. Once the reference frame is adjusted, the turbulence measurements can be analyzed as spatial signals or temporal signals.

A. Turbulent structure function

The second-order structure function is a spatial analysis technique used for profiles of turbulence, such as those collected by Acoustic Doppler Current Profilers (ADCPs). Following [3], the vertical second-order structure function $D(z,r)$ of velocity fluctuations $u'(z)$ is defined as

$$D(z,r) = \left\langle \left[u'(z) - u'(z+r)\right]^2 \right\rangle, \tag{2}$$

where z is the vertical location, r is the lag distance between velocity measurements, and the bracket denotes a time-average. A distinct feature of the structure function is that spatially uniform velocities are neglected in the calculation (i.e., only the variations in space matter). This makes the structure function very tolerant to sensor platform motion, because platform motion only introduces uniform offsets in velocity, at least along a given axis [4]. Furthermore, variance in time is not significant to the structure function, other than as contamination by non-stationarity, because it is the difference of $u'(z)$ over spatial scales r that controls $D(z,r)$.

The structure function of the turbulence is interpreted as a direct observation of the energy cascade that determines the dissipation rate of turbulent kinetic energy [5]. In terms of wavenumber k, the energy in a cascade of isotropic eddies is expected to follow a $k^{-5/3}$ dependence. This is often observed indirectly as a frequency $f^{-5/3}$ dependence via application of Taylor's frozen field hypothesis. For the structure function, this requires a power law $D(z,r) \sim u'^2 \sim r^{2/3}$ (equivalent to $k^{-5/3}$). Thus, calculated $D(z,r)$ are fit to

$$D(z,r) = A(z)r^{2/3} + N, \tag{3}$$

where an A is fitted for each z and N is an offset due to measurement noise (i.e., Doppler uncertainty, in the case of ADCPs).

Assuming homogenous turbulence and a cascade of isotropic eddies in the inertial subrange, the dissipation rate of turbulent kinetic energy scales as $\epsilon \sim u'^2/T \sim u'^3/r$, where T is a time scale given by r/u'. The slope $A(z)$ of the $r^{2/3}$ structure function is the related to the dissipation rate by

$$\epsilon(z) = \mathcal{C}_v^{-3} A(z)^{3/2}, \tag{4}$$

where $\mathcal{C}_v = 1.45$ is a constant [3].

SWIFT: Surface Wave Instrument Float with Tracking

Hull	Anodized aluminum
Power	14 VDC, Alkaline or Lithium D cell packs
Weight	30 kg in air
Dimensions	1.25 m draft, 1.0 m mast, 0.35 m diameter
Shipping crate	1.65 m length, 0.5 m width, 0.5 m depth
Endurance	20 days (Alkaline), 60 days (Lithium)
Tracking (RF)	Garmin Astro DC40 collars (10 km range)
Tracking (Iridium)	Geoforce SmartOne (global)
Telemetry	Iridium SBD
Processor	Sutron Xpert
Profiler	2 MHz Nortek Aquadopp HR
Met	Airmar PB200
IMU	Microstrain 3DM-GX3-35
CT	Aanderaa 4319
Camera	123 Camera Y201-TTL
Light	Yellow 1s strobe

Fig. 1. Picture and specifications for the Surface Wave Instrument Float with Tracking (SWIFT, v3).

B. Turbulent kinetic energy spectra

Turbulence measurements are more commonly analyzed as a temporal signal, using the Fast Fourier Transform (FFT) and standard spectral processing techniques. This is typically done using rapidly sampled ($>$ 10 Hz) Acoustic Doppler Velocimeter (ADV) data at a single point in space to obtain

$$S_{uu}(f) = \frac{|\mathcal{FFT}(u-\bar{u})|^2}{ndf}, \tag{5}$$

where n is the number of observations and df is the frequency bandwidth determined by the inverse of the time elapsed during the observations. Here, platform motion can interfere directly with the processing, if the platform motion introduces cyclic contaminations. If the motion is a constant offset, or drift, it is a trivial adjustment to $\bar{u}$.

Following Taylor's hypothesis, the turbulent kinetic energy (TKE) frequency spectra are converted to wavenumber spectra by assuming the advection of a frozen field [1], [6], [7]. The slope of the spectrum in the "inertial sub-range" represents the energy cascade that leads to turbulent dissipation. The dissipation rate is obtained by fitting an amplitude B to this portion of the spectra, $S_{uu}(f) = Bf^{-5/3}$, and taking

$$\epsilon = \left(\frac{B}{(\bar{u}/2\pi)^{2/3}\kappa}\right)^{3/2}, \tag{6}$$

where the Kolmogorov constant is $\kappa = 0.55$. ,

II. Wave following turbulence measurements

The Surface Wave Instrument Float with Tracking (SWIFT) was developed as an autonomous platform to make turbulence measurements in the wave-following reference frame [8]. For this platform, $\bar{u}$ is the time mean drift velocity measured by the changing GPS positions, $\tilde{u}$ are the wave orbital velocities measured by the phase-resolving GPS velocities, and u' are the turbulent fluctuations of velocity measured by a pulse-coherent ADCP (Nortek 2 MHz Aquadopp HR) that is mounted on the lower hull looking up and out towards the water surface.

Version 3 of the SWIFT is shown in Figure 1. This version includes onboard data processing and Iridium telemetry of hourly results, with a 90 day mission life. A key element is an IMU (MicroStrain 3DM-GX3-35) that integrates GPS positions and velocities to provide a complete Attitude Heading Reference System (AHRS). This is used to calculate wave energy spectra and directional moments, following [9].

The adaption of the structure function (Eqs. 2 to 4) for SWIFT measurements is described in [8] and adopts many of the processing details from [10]. The wave-following nature of the SWIFT platform is essential to measuring the strong turbulence in the crests of breaking waves, which are above the mean Eulerian (fixed) sea level. Velocity profiles are measured at 4 Hz, using beams that look out and up from the lower hull, in profiles that are 0.8 m long at 0.04 m resolution.

The wave-following motion of the SWIFT (or any floating body) is imperfect, and this introduces small contaminations in the calculation of $D(z,r)$.When the SWIFT heaves (i.e., bobs) relative to the wave-following surface, neighboring velocity bins are no longer fully independent, because the heaving motion moves the instrument relative to the bins. Similarly, when the SWIFT tilts, the projection of velocity bins shifts, and neighboring velocity bins overlap. The overlap will reduce the velocity differences in Eq. 2 and thus bias low the estimates of $D(z,r)$. The bias can be removed by applying a correction to the lag distances $r = r_0 - \Delta r$, such that

$$r = r_0 - \left(\frac{\sigma_z}{\cos\bar{\theta}}\right) - \left(\frac{z_0 - z}{2\cos^2\bar{\theta}}\bar{\theta}\sigma_\theta\right), \tag{7}$$

where the first term is the original lag distance r_0, the second term is the correction for heave in vertical position z, and the third term is the correction for tilting in the beam angle θ. Corrections are made using the measured deviations from prefect wave following motion: σ_z is the standard deviation of the Aquadopp distance z_0 beneath the wave following surface (measured by the onboard pressure gage) and σ_θ is the standard deviation of beam angle θ in radians (inferred from the onboard orientation sensor). Using typical values of $\sigma_z = 0.01$ m and $\sigma_\theta = 0.09$ rad ($= 5$ deg), the typical correction is $\Delta r \sim 0.03$ m, which is small relative to the $\mathcal{O}(0.5)$ m lag distances used to determine $D(z,r)$. Finally, it must be noted that the triangular bin weighting used in Nortek's processing also results in some overlap in velocity information between neighboring bins, but that offset is not treated by Eq. 7.

Examples of the structure function $D(z,r)$, the fits $A(z)r^{2/3}$ at each z, and the resulting profile of $\epsilon(z)$ are shown in Figure 2, using data collected during a winter storm on Lake Washington. For each depth z, there are trends for increased velocity differences with increasing lag distances r, and the slopes of these trends differ by vertical location beneath the wave-following surface. These trends are consistent with a cascade of turbulent kinetic energy from large to small eddies, and this is reflected in the decay of ϵ with depth beneath the surface.

The offset N in the structure function is expected to be $2\sigma_{u'}^2$, in which $\sigma_{u'}$ is the Doppler noise of the velocity measurement [3], [11]. The Doppler noise contributes additional differences between velocity measurements uniformly across all lag distances, and thus will produce a positive offset to $D(z,r)$. Here, N values are obtained as a free parameter in the fits (rather than prescribed) and are used to evaluate errors

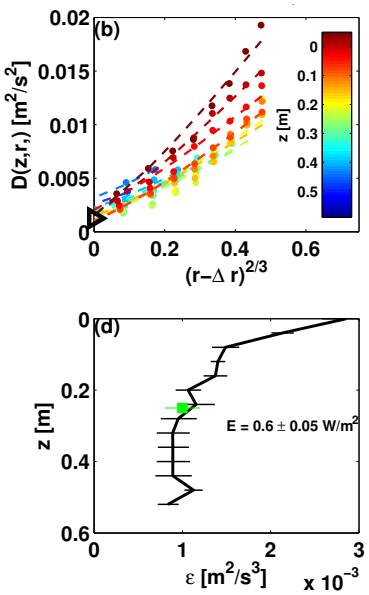

Fig. 2. Top: the turbulent structure function at different depths (indicated by color) beneath the wave-following surface. Bottom: the resulting depth profile of turbulent dissipation rate. The green symbol is an independent estimate of the dissipation rate, using an ADV temporarily added to the SWIFT and applying the spectral method (Eq. 6.

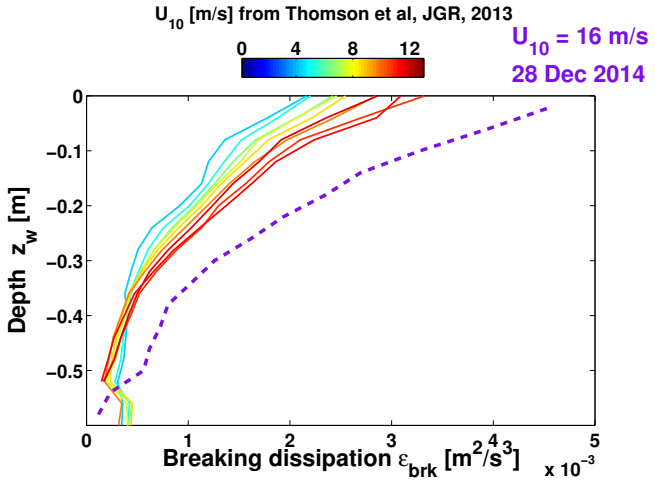

Fig. 3. Turbulent dissipation rate profiles within wave crests, colored by wind speed. The purple curve is an addition of new data, at higher wind speed, since the publication of [15].

in the methods or violations in the assumptions. Specifically, the N values are examined for a normal distribution (i.e., no bias). In the example, the noise intercepts N are similar or less than the predicted $2\sigma_{u'}^2$ value, which is shown by an open triangle on the vertical axis Figure 2.

To date, SWIFTs have been used to measure turbulent dissipation from breaking waves in the open ocean [12], at a tidal inlet [13], at the offshore front of a river plume [14], and in the marginal ice zone. Results from the open ocean measurements are shown in Figure 3, including new measurements since the publication of [12]. The profiles of TKE dissipation rate beneath wave crests are clearly sorted by wind speed, which is related to the dynamics of an equilibrium balance between wind input to waves and dissipation by breaking.

III. Moored Turbulence Measurements

The Tidal Turbulence Mooring (TTM) was developed to measure turbulence at mid-water positions in fast moving currents [15]. The primary motivation was for turbulence characterization at potential tidal energy sites, where direct measurements at hub-height (nominally 10 m above the seabed) are required to inform turbine design. Bottom-mounted Acoustic Doppler Current Profilers are unable to capture the smaller length scales, because of the divergent beams, and thus Acoustic Doppler Velocimeters (ADVs) must be placed at hub-height positions. The TTM is a compliant mooring that is an alternative to deploying 10 m tripods in high currents for placement of ADVs. The key to the success of the mooring is the prevention (via streamlined design) and correction (via post-processing) of contamination in velocity measurements by the mooring motion itself.

The TTM design is shown in Figure 4. Primary components are an anchor, a buoyant float rated for sub-surface use, and an instrument vane. ADV(s) are mounted to the instrument vane and the mooring line is wrapped in filaments to prevent strumming. The mooring has swivels at each junction, such that the vane can yaw passively and always face the principal component of the flow (which is important for tidal sites). Drag forces cause the mooring to lean, or 'blow down', in strong currents, and tether lengths must be longer than the desired depth to account this.

The TTM has been deployed a total for four times: in Admiralty Inlet (Puget Sound, WA, USA) in June 2012, Sept 2012, and June 2014, and in Chacao Channel (Chile) in February 2013. Various data from these deployments are used to demonstrate the methods and provide an example of the results. In all cases, raw ADV data are collected at 32 Hz.

A. Motion correction of ADV data

Velocity measurements are made with Nortek Vector ADVs equipped with MicroStrain 3DM-GX3-25 inertial motion sensors (IMU), which are recently available as an optional upgrade to the Vector. This records ADV orientation and all 6 degrees of motion (3 rotation, 3 acceleration) synchronous with each velocity measurement. [15] showed that mooring motion can effectively be removed from the TKE spectrum using quasi-synchronous IMU measurements and subtracting the spectrum of motion from the spectrum of raw velocities, provided that cross-spectrum of the signals is also removed. [16] showed that synchronous IMU-ADV measurements can be used to remove mooring motion in the time-domain. The time domain method is preferred, because the corrected time series enables a much fuller range of calculations (beyond simply the TKE spectrum).

The time-domain correct is made in post-processing via

$$\vec{u}(t) = \vec{u}_{ADV}(t) + \vec{u}_M(t). \quad (8)$$

Here $\vec{u}_{ADV}$ is the uncorrected (raw) ADV velocity signal and $\vec{u}_M$ is the ADV sensor's motion. Note that velocities are added in Eq. 8, not subtracted, because the motion-induced velocity measured by the ADV has the opposite sign as the mooring

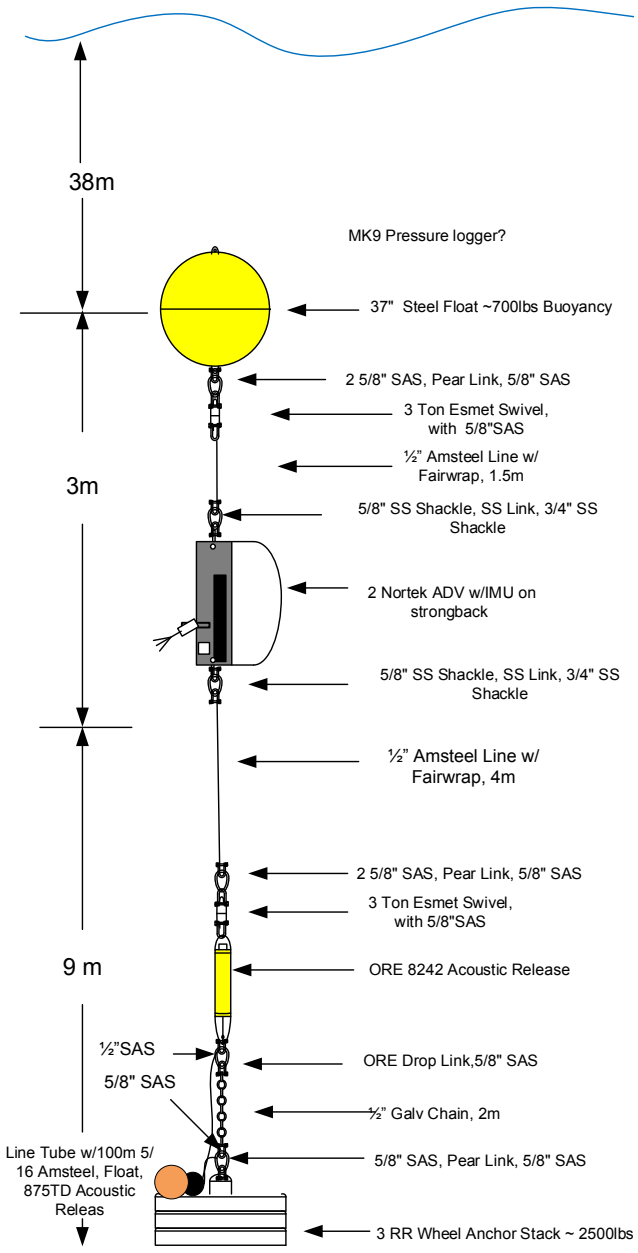

Fig. 4. Schematic of the Tidal Turbulence Mooring (TTM).

motion itself. $\vec{u}_M$ is computed from the IMU rotation rate vector ($\vec{\omega}$) and linear-acceleration ($\vec{a}$) as,

$$\vec{u}_m(t) = \vec{\omega}(t) \times \vec{\ell} + \int \vec{a}'(t)\mathrm{d}t \quad , \tag{9}$$

where ℓ is the vector from the IMU to the ADV sensor-head and $\vec{a}'$ is the high-pass filtered IMU acceleration and all quantities are in the earth-frame (rotated using the time-dependent IMU-supplied orientation matrix). Finally, all velocity signals are rotated into a right-handed principal axes coordinate system such that u, x are aligned with the ebb-flood direction ($+u, +x$: ebb), v, y the cross-stream direction and $+w, +z$ the vertical-up direction.

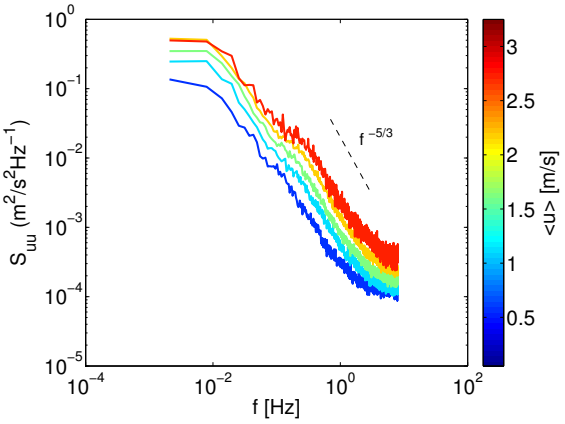

Fig. 6. Results from the Tidal Turbulence Mooring: Turbulent Kinetic Energy density versus frequency. Colors indicate the mean flow speed $< u >$ at each stage of the tide. Black dashed line shows the expected slope of the inertial sub-range.

While spectra of $\vec{u}_{ADV}$ have peaks that indicate motion contamination (Figure 5), motion correction removes the vast majority of this contamination such that the u, v and w motion-corrected spectra have similar amplitude and have a $f^{-5/3}$ slope in the inertial sub-range [5]. The v-component spectra has a persistent motion-contamination peak due to the large amplitude of the sensor-motion in that direction, but it seams reasonable to interpolate over this peak when estimating the v-component spectra. This suggests that motion corrected moored ADV measurements can provide reasonable estimates of the TKE spectrum.

TKE spectra are computed using a fast Fourier transform (FFT) of 5-minute detrended, hanning-windowed segments with 50% overlap. The spectra $S_{uu}(f)$ are then grouped by mean velocity to obtain spectra with approximately 20 degrees of freedom.

Results from the Chacao Channel (Chile) are shown in Figure 6. Valid TKE spectra are recovered from the mooring in currents up to 3 m/s. The spectra are well sorted by mean velocity $< u >$, because turbulence levels are correlated with mean flow speeds. These spectra can be used to estimate the turbulent dissipation rate ϵ via Eq. 6, as shown in Figure 7 as a function of mean tidal flow. The ϵ values follow the expected u^3 scaling for all except the slowest mean flows.

Frequency spectra such those in Figure 6 can also be used to qualify the scales of variations that will affect tidal turbines at this site. Given a spectral response function for a turbine, this information could be used in high-fidelity modeling of turbine performance and loading.

IV. Conclusion

Recent advances in IMU sensors make it possible to measure turbulence in the ocean from moving platforms. The platform motion can be an advantage, as in the case of a floating buoy to measure turbulence in breaking wave crests, or a source of contamination, as in the case of a compliant mooring. In both cases, tracking and correction of motion can be performed sufficiently to enable spatial and temporal processing to obtain the turbulent dissipate rate.

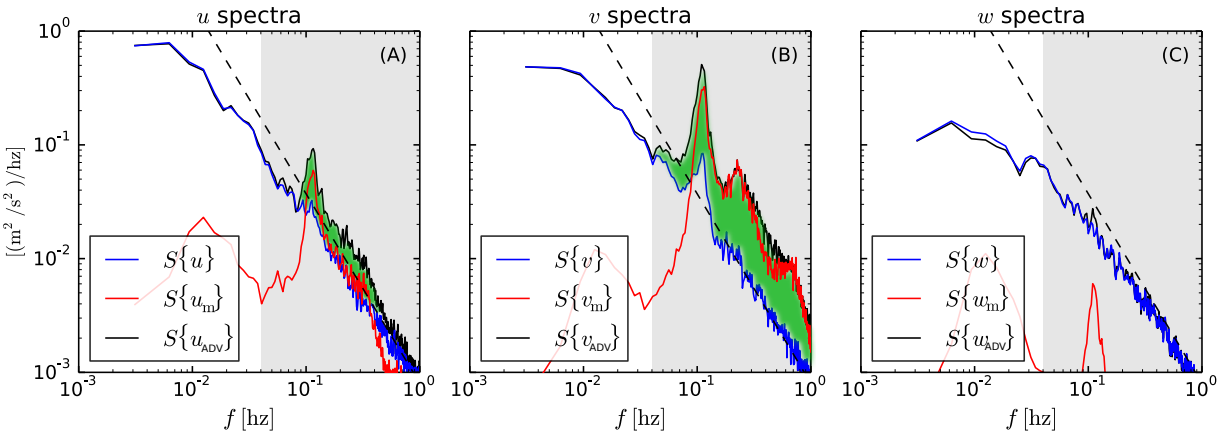

Fig. 5. Velocity spectra from a single ADV on a TTM, A: u-component, B: v-component, C: w-component). Spectra are of uncorrected velocity measurements ($\vec{u}_{ADV}$, black), ADV-head motion ($\vec{u}_M$, red), and motion-corrected velocity ($\vec{u}$, blue). Green shading indicates the influence of motion correction. The gray-shaded region indicates the isotropic 'inertial sub-range'.

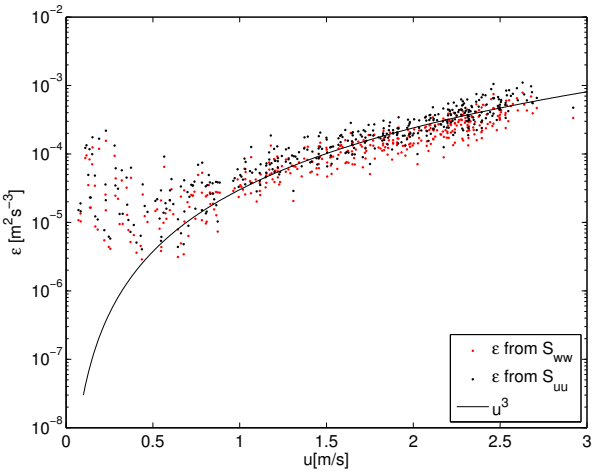

Fig. 7. Turbulent dissipation rates from the TMM versus mean tidal flow. Dissipation rates follow the expected u^3 scaling for all except the slowest mean flows.

ACKNOWLEDGMENT

The authors would like to thank Capt. Andy Reay-Ellers of the R/V Jack Robertson and Eduardo Hernandez of the R/V Jurgen Winter. This work was funded by the Office of Naval Research, the National Science Foundation, and the U.S. Dept. of Energy.

REFERENCES

[1] J. L. Lumley and E. A. Terray, "Kinematics of turbulence convected by a random wave field," *J. Phys. Oceanogr.*, vol. 13, pp. 2000–2007, 1983.

[2] E. A. D'Asaro, D. M. Farmer, J. T. Osse, and G. T. Dairiki, "A lagrangian float," *Journal of Atmospheric and Oceanic Technology*, vol. 13, no. 6, pp. 1230–1246, 2014/05/01 1996. [Online]. Available: http://dx.doi.org/10.1175/1520-0426(1996)013¡1230:ALF¿2.0.CO;2

[3] P. Wiles, T. P. Rippeth, J. Simpson, and P. Hendricks, "A novel technique for measuring the rate of turbulent dissipation in the marine environment," *Geophys. Res. Let.*, vol. 33, p. L21608, 2006.

[4] N. S. Lucas, J. H. Simpson, T. P. Rippeth, and C. P. Old, "Measuring turbulent dissipation using a tethered adcp," *Journal of Atmospheric and Oceanic Technology*, vol. 31, no. 8, pp. 1826–1837, 2014/08/08 2014. [Online]. Available: http://dx.doi.org/10.1175/JTECH-D-13-00198.1

[5] A. N. Kolmogorov, "Dissipation of energy in the locally isotropic turbulence," *Dokl. Akad. Nauk SSR*, vol. 30, pp. 301–305, 1941.

[6] J. Trowbridge and S. Elgar, "Turbulence measurements in the surf zone," *J. Phys. Oceanogr.*, vol. 31, pp. 2403–2417, 2001.

[7] F. Feddersen, "Quality controlling surf zone acoustic doppler velocimeter observations to estimate the turbulent dissipation rate," *J. Atmos. Ocean. Tech.*, vol. 27, no. 12, pp. 2694–2696, 2010.

[8] J. Thomson, "Wave breaking dissipation observed with SWIFT drifters," *Journal of Atmospheric and Oceanic Technology*, vol. 29, no. 12, pp. 1866–1882, 2013/01/03 2012. [Online]. Available: http://dx.doi.org/10.1175/JTECH-D-12-00018.1

[9] T. H. C. Herbers, P. F. Jessen, T. T. Janssen, D. B. Colbert, and J. H. MacMahan, "Observing ocean surface waves with GPS tracked buoys," *J. Atmos. Ocean. Tech.*, vol. 29, 2012.

[10] J. Gemmrich, "Strong turbulence in the wave crest region," *J. Phys. Oceanogr.*, vol. 40, pp. 583–595, 2010. [Online]. Available: DOI: 10.1175/2009JPO4179.1

[11] P. J. Rusello and E. Cowen, "Turbulent dissipation estimates from pulse coherent doppler instruments." in *Current, Waves and Turbulence Measurements (CWTM)*, 2011.

[12] J. Thomson, E. A. D'Asaro, M. Cronin, E. Rogers, R. Harcourt, and A. Schcerbina, "Waves and the equilibrium range at Ocean Weather Station P," *J. Geophys. Res.*, vol. 118, pp. 1–12, 2013.

[13] S. Zippel and J. Thomson, "Wave breaking and turbulence at a tidal inlet," *J. Geophys. Res.*, accepted.

[14] J. Thomson, A. R. Horner-Devine, S. Zippel, C. Rusch, and W. Geyer, "Wave breaking turbulence at the offshore front of the columbia river plume," *Geophysical Research Letters*, pp. n/a–n/a, 2014. [Online]. Available: http://dx.doi.org/10.1002/2014GL062274

[15] J. Thomson *et al.*, "Tidal turbulence spectra from a compliant mooring," in *Proceedings of the 1st Marine Energy Technical Symposium (METS)*, April 2013.

[16] L. Kilcher, J. Thomson, and J. Colby, "Determing the spatial coherence of turbulence at MHK sites," in *Proceedings of the 2nd Marine Energy Technical Symposium (METS)*, ', Ed., April 2014.